Title

ACE2 Receptor-Modified Algae-Based Microrobot for Removal of SARS-CoV-2 in Wastewater.

Journal

Journal of the American Chemical Society, 143(31)

ISSN

0002-7863

Authors

Zhang, Fangyu
Li, Zhengxing
Yin, Lu
et al.

Publication Date

2021-08-01

DOI

10.1021/jacs.1c04933

Peer reviewed

JACS
JOURNAL OF THE AMERICAN CHEMICAL SOCIETY
pubs.acs.org/JACS
Article

ACE2 Receptor-Modified Algae-Based Microrobot for Removal of SARS-CoV-2 in Wastewater

Fangyu Zhang,[#] Zhengxing Li,[#] Lu Yin, Qiangzhe Zhang, Nelly Askarinam, Rodolfo Mundaca-Uribe, Farshad Tehrani, Emil Karshalev, Weiwei Gao, Liangfang Zhang,* and Joseph Wang*

Cite This: https://doi.org/10.1021/jacs.1c04933
Read Online
ACCESS | Metrics & More | Article Recommendations | Supporting Information

ABSTRACT: The coronavirus SARS-CoV-2 can survive in wastewater for several days with a potential risk of waterborne human transmission, hence posing challenges in containing the virus and reducing its spread. Herein, we report on an active biohybrid microrobot system that offers highly efficient capture and removal of target virus from various aquatic media. The algae-based microrobot is fabricated by using click chemistry to functionalize microalgae with angiotensin-converting enzyme 2 (ACE2) receptor against the SARS-CoV-2 spike protein. The resulting ACE2-algae-robot displays fast (>100 μm/s) and long-lasting (>24 h) self-propulsion in diverse aquatic media including drinking water and river water, obviating the need for external fuels. Such movement of the ACE2-algae-robot offers effective "on-the-fly" removal of SARS-CoV-2 spike proteins and SARS-CoV-2 pseudovirus. Specifically, the active biohybrid microrobot results in 95% removal of viral spike protein and 89% removal of pseudovirus, significantly exceeding the control groups such as static ACE2-algae and bare algae. These results suggest considerable promise of biologically functionalized algae toward the removal of viruses and other environmental threats from wastewater.

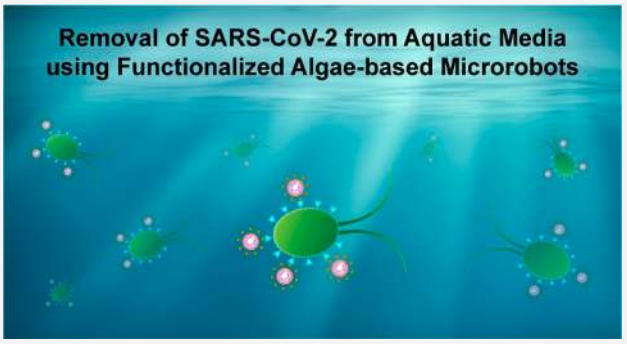

INTRODUCTION

As an emerging coronavirus associated with formidable infectiousness and lethality, severe acute respiratory syndrome coronavirus 2 (SARS-CoV-2) can spread through multiple transmission routes, including direct airborne transmission from respiratory droplets or aerosols and indirect fomite transmission upon contacting contaminated subjects or surfaces.[1] While SARS-CoV-2 is known to infect the respiratory tract, it can also infect the gastrointestinal tract with a prolonged residence in fecal samples.[2] In addition to its presence in stool samples, SARS-CoV-2 has also been detected in domestic wastewater in sewage and downstream rivers.[3−5] These reports have raised concerns that wastewater could be a potential route of SARS-CoV-2 infection via fecal-oral transmission.[6,7] To minimize the risk of secondary transmission to humans, there remains an urgent need to develop wastewater treatment strategies for the effective removal of SARS-CoV-2. Several physical, chemical, and biological processes, including sedimentation, filtration, disinfection with UV or oxidants, and enzymatic degradation, have been proposed to tackle SARS-CoV-2 decontamination in wastewater.[8] While these conventional wastewater purification approaches are effective in general, it is still necessary to explore new techniques that are easy, fast, and effective in resolving the wastewater contamination issue of SARS-CoV-2.

We present here a biohybrid microrobot for the efficient removal of SARS-CoV-2 from contaminated aquatic media. Because of their robust self-propulsion ability and facile surface functionalization, microrobots offer a dynamic and powerful strategy for rapid decontamination of water matrices from a wide range of environmental pollutants, including dyes,[9,10] heavy metals,[11,12] oil,[13] pathogenic organisms,[14,15] nitroaromatic explosives,[16] and chemical and biological warfare agents.[17] Such movement of functional microrobots provides an enhanced collision/contact and adsorption of the target contaminants along with localized self-mixing as compared to their static counterparts, thus enabling efficient and rapid decomposition and accelerated "on-the-fly" removal of pollutants.[18,19] However, widespread environmental and defense applications of current synthetic microrobotic platforms have been hampered by their short life span, need for toxic fuels, or complex external actuation equipment, and restricted operating media. To address these challenges faced

Received: May 12, 2021

https://doi.org/10.1021/jacs.1c04933
J. Am. Chem. Soc. XXXX, XXX, XXX−XXX

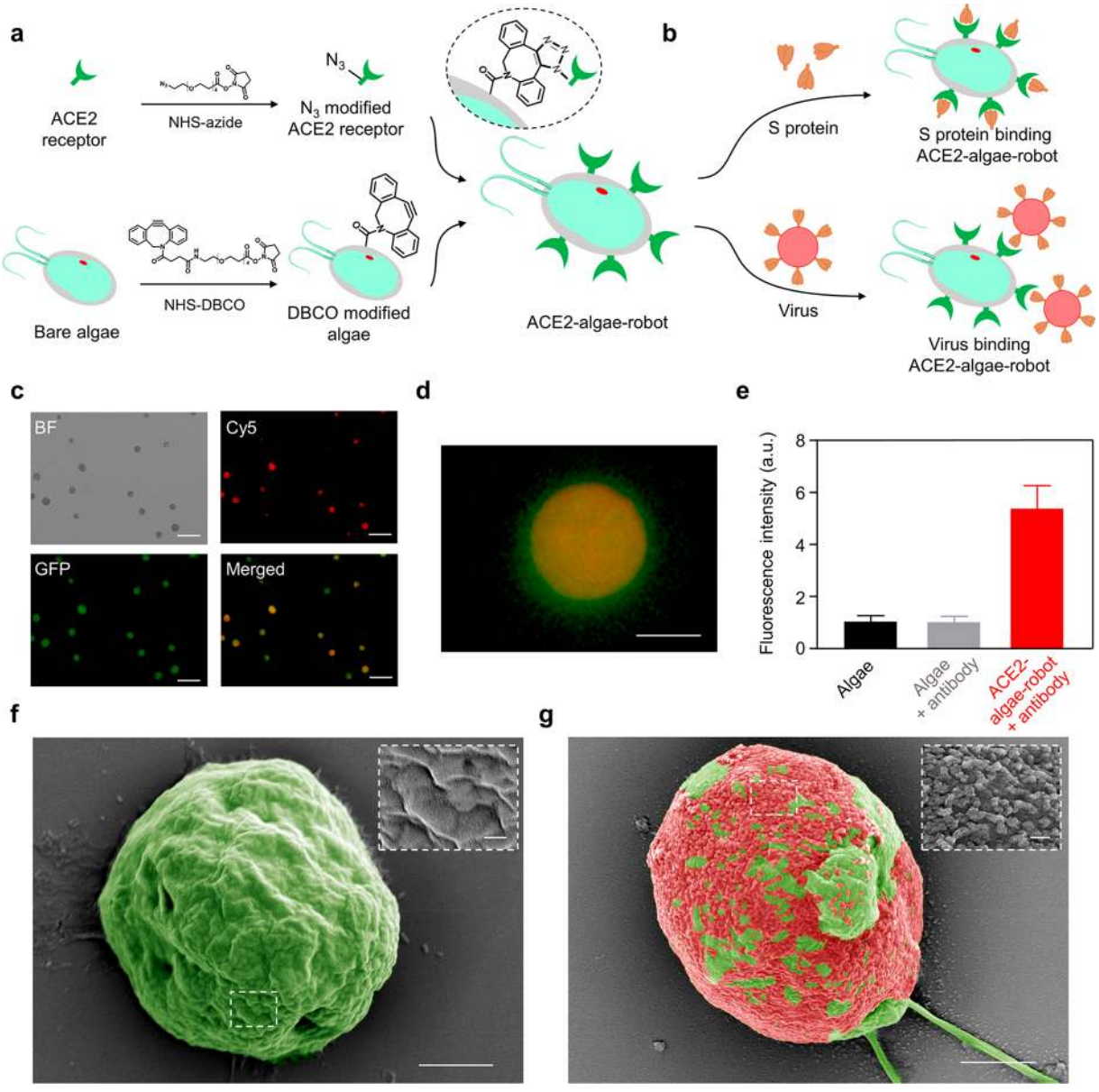

Figure 1. Fabrication and characterization of ACE2-functionalized algae microrobot (denoted "ACE2-algae-robot"). (a) Schematic of the functionalization of microalgae with ACE2 receptor. (b) Schematic depicting the use of the ACE2-algae-robot for the binding and removal of spike protein and SARS-CoV-2 virus. (c) Brightfield, fluorescent, and merged images of the ACE2-algae-robot after immunostaining. Autofluorescence of natural algae chloroplast in Cy5 channel; immunostaining of Fluor488-conjugated anti-ACE2 antibody in GFP channel. Scale bar: 50 μm. (d) Enlarged fluorescence image from panel (c) clearly shows the full coverage of the ACE2 receptor onto the algae surface. Red core: chloroplast of the algae; green: Fluor488-conjugated anti-ACE2 antibody. Scale bar: 5 μm. (e) GFP fluorescence intensity of bare algae, bare algae with Fluor488-conjugated anti-ACE2 antibody, and the ACE2-algae-robot with Fluor488-conjugated anti-ACE2 antibody. (f,g) Pseudocolored scanning electron microscopy (SEM) images of the ACE2-algae-robot (f) before and (g) after contact with the virus. Green: ACE2-algae-robot; red: SARS-CoV-2 pseudovirus. Scale bar: 2 μm. Zoom-in images show the surface morphology of the ACE2-algae-robot (f) before and (g) after contact with the virus. Scale bar: 200 nm.

by synthetic microrobots, biohybrid microrobots, combining self-propelled microorganisms with functional biomaterials, have recently demonstrated significant promise for large-scale environmental remediation.[20−22]

The new microrobotic strategy for SARS-CoV-2 removal relies on angiotensin-converting enzyme 2 (ACE2) receptor functionalized algae microrobot (denoted "ACE2-algae-robot"). The ACE2 receptor is responsible for the recognition of the target virus with a high binding affinity to the S1 subunit of the viral spike protein and has been reported as an effective cellular receptor for SARS-CoV-2 toward diverse virus-related sensing,[23] therapeutic,[24] and neutralization[25] applications. Algae have been used for wastewater treatment[26] but not in connection to active microrobots or toward the management of SARS-CoV-2 contaminated water. Here we select *Chlamydomonas reinhardtii* as a model algae because of their attractive properties, including easy large-scale production, fast motion in diverse aqueous environments, long life span, and facile surface functionalization.[27,28] As illustrated in Figure 1a, the ACE2-algae-robot is fabricated using a click chemistry reaction for anchoring the ACE2 receptor onto the algae surface. The resulting ACE2-algae-robot displays fast move-

https://doi.org/10.1021/jacs.1c04933
J. Am. Chem. Soc. XXXX, XXX, XXX−XXX

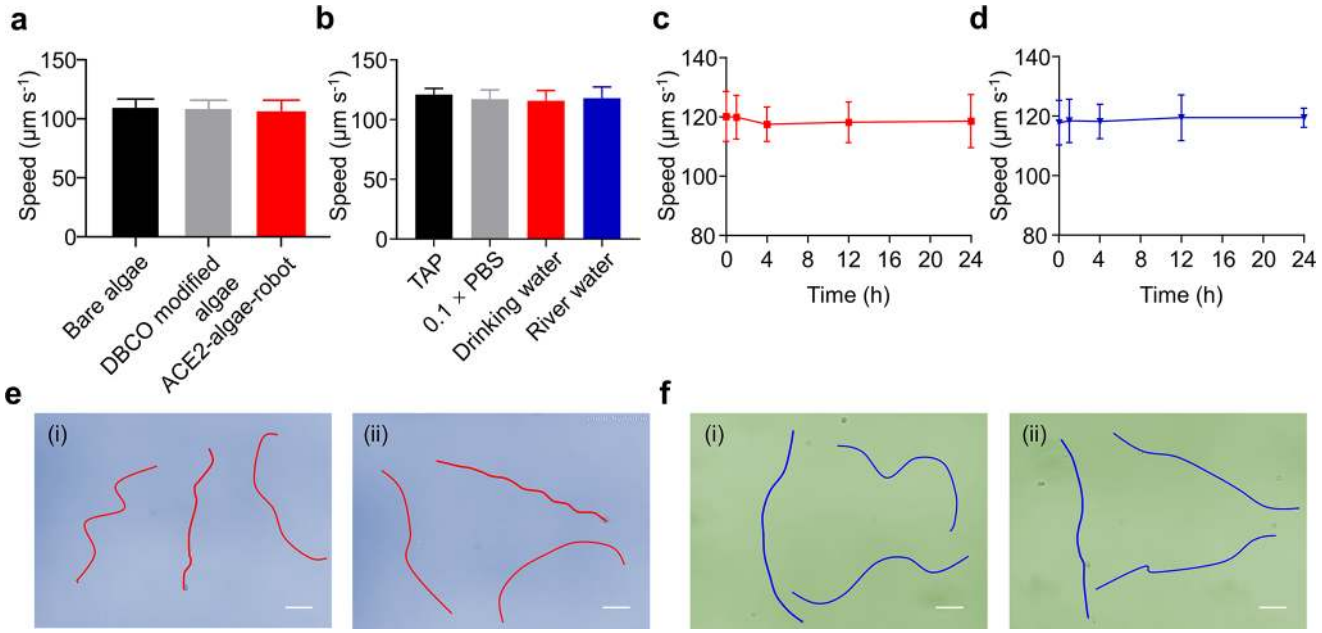

Figure 2. Motion behavior of the ACE2-algae-robot. (a) Effect of the algae functionalization upon its swimming behavior: speeds of bare algae, DBCO-modified algae, and the ACE2-algae-robot (n = 6; mean + s.d.). (b) Movement of the ACE2-algae-robot in different media: tris-acetate-phosphate medium (TAP), 0.1 × phosphate-buffered saline (PBS; diluted from 1 × PBS with DI water), drinking water, and river water (n = 6; mean + s.d.). (c,d) Speed of the ACE2-algae-robot at different time points (0, 1, 4, 12, and 24 h) in (c) drinking water and (d) river water (n = 6; mean ± s.d.). (e,f) Representative optical trajectories of the movement of the ACE2-algae-robot over 2.5 s motion in (e) drinking water and (f) river water obtained at (i) 0 h and (ii) 24 h. Scale bar: 40 μm.

ment (>100 μm/s) in various media, without compromising the intrinsic mobility of unmodified algae. Using SARS-CoV-2 spike protein (S protein) and pseudovirus as model contaminants, the moving ACE2 receptor on the algae surface leads to remarkable binding to the targets, enabling about 95% removal of the S protein and about 89% removal of SARS-CoV-2 pseudovirus from various testing wastewater (Figure 1b). The pseudovirus bears the same spike protein as the live SARS-CoV-2 virus and has been shown extremely useful for developing SARS-CoV-2 detection and neutralization technologies.[29] These results clearly illustrate the feasibility of using the biohybrid microrobot for large-scale "on-the-fly" decontamination of coronavirus and possibly other diverse environmental threats in wastewater.

RESULTS AND DISCUSSION

Fabrication and Characterization of the ACE2-Algae-Robots. Figure 1 schematically displays (a) the fabrication process of the ACE2 modified algae and (b) the targeting and removal of S protein and SARS-CoV-2 pseudovirus from wastewater. In the study, the ACE2 receptors were conjugated to the algae surface using a click chemistry approach. Specifically, the azide and dibenzocyclooctyne (DBCO) groups were conjugated to the ACE2 receptors and the algae, respectively, via the *N*-hydroxysuccinimide (NHS) ester reaction. The conjugated N_3 on the ACE2 receptors will then react effectively with the DBCO on the algae, resulting in the formation of the ACE2-algae-robot. Next, immunostaining was performed to visualize the ACE2 receptors attached on the algae surface. Here, Fluor488-conjugated anti-ACE2 antibody was used to label the ACE2 receptors on the algae. As illustrated in Figure 1c, the signals from immunostaining of fluorescent anti-ACE2 antibody in the GFP channel colocalized with those of the autofluorescence of algae in the Cy5 channel. The enlarged image in Figure 1d further indicates the coverage of ACE2 receptors on the algae surface. In addition, the unmodified algae incubated with fluorescent anti-ACE2 antibody exhibited a negligible change of GFP fluorescence intensity as compared to the bare algae alone (Figure 1e and Figure S1). In contrast, the ACE2-algae-robot incubated with fluorescent anti-ACE2 antibody showed a significant increase in fluorescent intensity as compared to the two control groups, reflecting the effective conjugation of ACE2 receptors onto the algae via click chemistry. The pseudocolored scanning electron microscopy (SEM) images further illustrate the ACE2-algae-robot before (Figure 1f and Figure S2i) and after (Figure 1g and Figure S2ii) contact with SARS-CoV-2 pseudovirus. The bound virus particles can be clearly observed on the ACE2-algae-robot from the inset of SEM images in Figure 1g.

Motion Behavior of ACE2-Algae-Robots in Aquatic Media. We next investigated the motion behavior of the biohybrid microrobot. After confirming the DBCO-NHS ester conjugation (Figure S3), the ACE2-algae-robot was fabricated by mixing DBCO modified algae with the azide-ACE2 receptor in DI water for 2 h. The speed of the DBCO-modified algae and the ACE2-algae-robot were measured to be 112 μm/s and 108 μm/s (~11 body length/s), respectively, compared to 115 μm/s of the bare algae, indicating that the functionalization process has a negligible effect on the motion of the algae (Figure 2a and Video S1). Once prepared in DI water, the ACE2-algae-robot was transferred into various aqueous media to test their mobility. As illustrated in Figure 2b and Video S2, the ACE2-algae-robot displayed efficient motion (>100 μm/s) in TAP medium, 0.1 × PBS, drinking water, and river water without a need of any external fuel to propel the robot. In addition, the ACE2-algae-robot demonstrated long-lasting motion in both drinking and river water matrices (Figure

https://doi.org/10.1021/jacs.1c04933
J. Am. Chem. Soc. XXXX, XXX, XXX−XXX

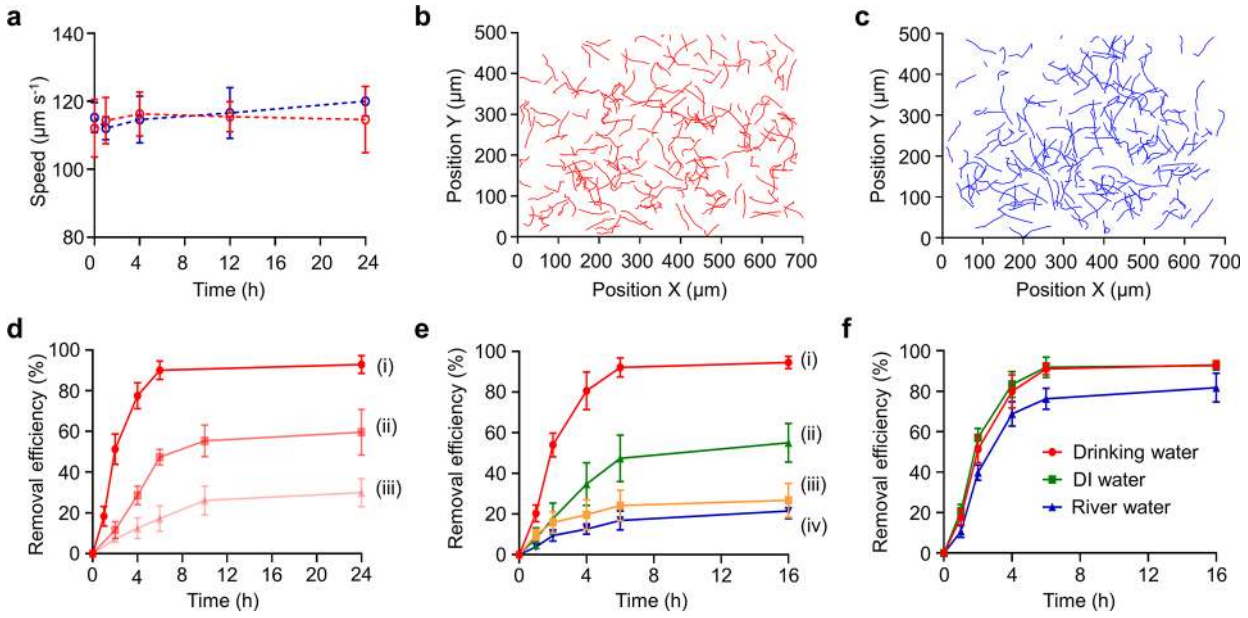

Figure 3. Use of the ACE2-algae-robot for the removal of SARS-CoV-2 spike protein. (a) Speed comparison of the ACE2-algae-robot in drinking water (red) and river water (blue) containing the spike protein (n = 6; mean ± s.d.). (b,c) Motion trajectory of the ACE2-algae-robot in (b) drinking water and (c) river water samples containing the spike protein. (d) Effect of the ACE2-algae-robot density on the spike protein removal kinetic profile in the drinking water. Algae input density: (i) 5×10^7 ml^{-1}, (ii) 2×10^7 ml^{-1}, and (iii) 5×10^6 mL^{-1} (n = 3; mean ± s.d.). (e) Kinetic profile of the spike protein removal efficiency from drinking water with the treatment of the (i) ACE2-algae-robot, (ii) bare algae, (iii) static ACE2-algae, or (iv) cell wall deficient algae. (f) Kinetic profile of the spike protein removal efficiency by employing the ACE2-algae-robot in different media, including drinking water, DI water, and river water (n = 3; mean ± s.d.).

2c,d and Video S3), indicating its capability for extended operation toward the removal of SARS-CoV-2 S protein and pseudovirus. The images in Figure 2e,f (along with Videos S4 and S5) illustrate representative tracking trajectories of the individual ACE2-algae-robot, over a 2.5 s interval, at different times [0 h (i) and 24 h (ii)] in drinking and river water, respectively, reflecting the highly stable algae motion in these media.

Removal of SARS-CoV-2 Spike Protein by ACE2-Algae-Robots. Figure 3a illustrates that the presence of viral S protein in the drinking water (red) and river water (blue) did not affect the mobility or the lifespan of the ACE2-algae-robot, which showed highly stable motion in both media for over 24 h operation. This was supported by the tracking trajectories of about 200 individual ACE2-algae-robots (during 0.6 s) after moving for 24 h in drinking water and river water, respectively (Figure 3b,c). The corresponding speed distribution indicates that 80% of algae moved faster than 100 μm/s (Figure S4). Such fast and continuous motion of the ACE2-algae-robot could accelerate its collision with viral S protein and thus improve the specific binding and removal of the target protein. Figure 3d examines the effect of ACE2-algae-robot density on the kinetic removal efficiency of S protein from drinking water. As expected, the speed and efficiency of the removal process increased upon increasing the density of the microrobots, with 5×10^7 ml^{-1} ACE2-algae-robot removing 95% of 2.88 ng/mL S protein from the water sample within 6 h. To compare the S protein removal capability between different algae groups, the same density of algae (5×10^7 ml^{-1}) from different control groups, including the ACE2-algae-robot, static ACE2-algae (deflagellated algae with the ACE2 receptor modification), bare algae, and cell wall deficient algae, was added to 500 μL drinking water containing 2.88 ng/mL S protein. The ACE2-algae-robot shows highly efficient binding and 95% removal efficiency after 6 h continuous motion (Figure 3e,(i). In comparison, the active bare algae lacking ACE2 (Figure 3e,(ii) and static ACE2-algae (Figure 3e,(iii) displayed only 46% and 23% removal efficiency after 16 h operation, respectively, indicating the critical role of the ACE2 receptor modification and algae motion on the speed and efficiency of the S protein removal. The S protein removal by the bare algae is likely attributed to nonspecific binding associated with the presence of diverse functional groups (e.g., carboxyl or amino groups) on the algae surface.[30] The images shown in Figure S5 represent a homogeneous mixture of the ACE2-algae-robot and S protein after 6 h incubation compared to clear sediment of static ACE2-algae after 6 h incubation. These results explain further the fast and efficient removal using the ACE2-algae-robot in Figure 3e. The ACE2-algae-robot also exhibits effective S protein removal in various media, including DI water, drinking water, and river water, as indicated by the similar kinetic profiles in Figure 3f. These results reveal that the ACE2-algae-robot, with long-lasting motion and ACE2 receptor for S protein recognition, represents an attractive system to enhance environmental remediation in complex aqueous surroundings.

Removal of SARS-CoV-2 Pseudovirus by ACE2-Algae-Robots. Following the effective removal of viral S protein, the next set of experiments examined the ability of the ACE2-algae-robot to remove SARS-CoV-2 pseudoviruses, which represents an effective alternative of live human SARS-CoV-2 virus for research to evaluate new antiviral technologies.[29] Figure 4a schematically illustrates the efficient removal of the SARS-CoV-2 pseudovirus from water samples using the ACE2-algae-robot. After ACE2-algae-robot treatment, the pseudoviruses are largely captured and removed from the solution, validated, and visualized by an NL-20 cell-based assay. The NL-20 cells remained nonfluorescent following 24 h

https://doi.org/10.1021/jacs.1c04933
J. Am. Chem. Soc. XXXX, XXX, XXX−XXX

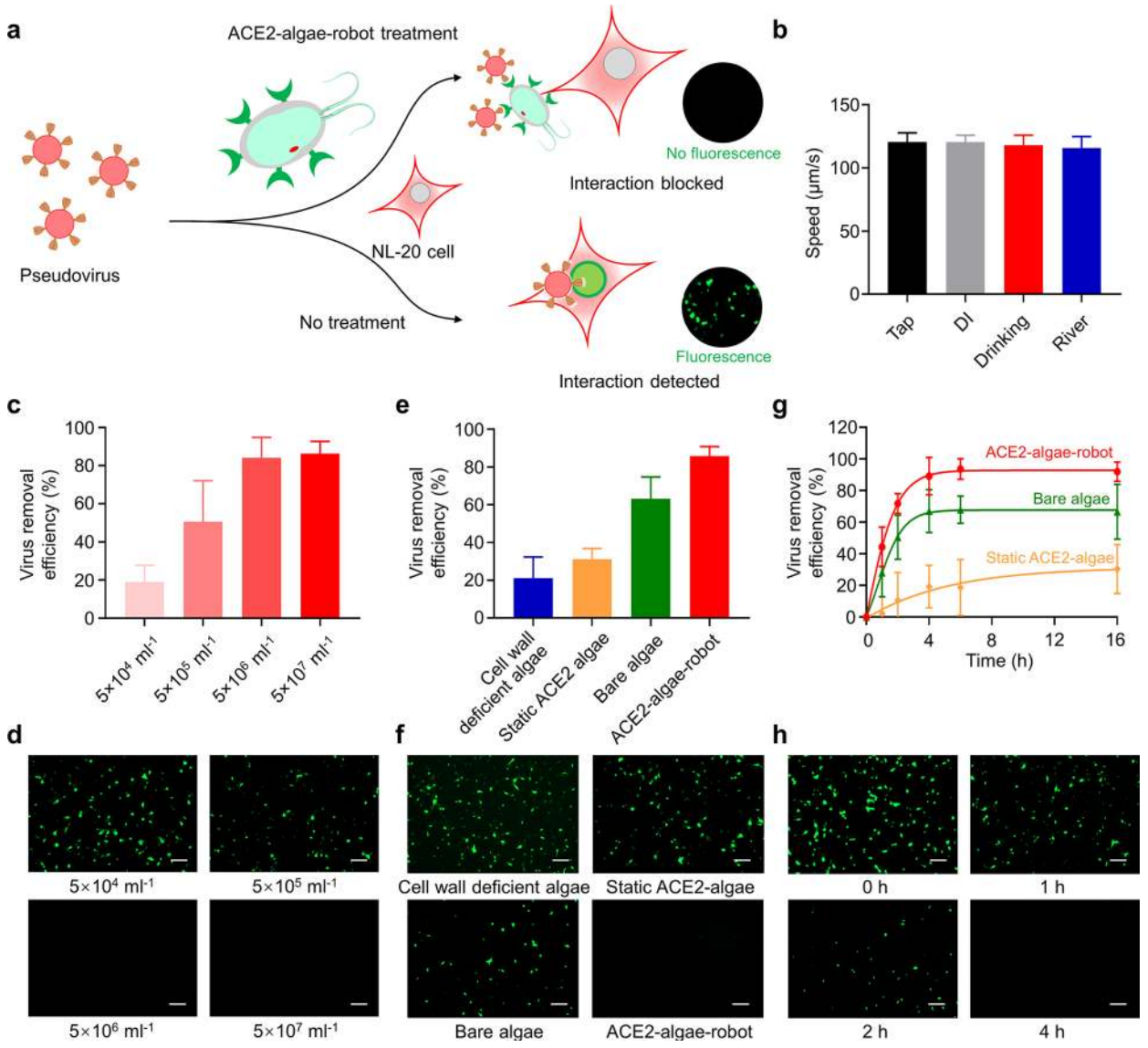

Figure 4. Use of the ACE2-algae-robot for the removal of SARS-CoV-2 pseudovirus. (a) Schematic illustrating the viral removal by the ACE2-algae-robot, which blocks the virus from entering cells. Inset: viral infection was indicated by expression of green fluorescent protein, whereas the virus treated by the ACE2-algae-robot shows low viral infection. (b) Speed comparison of the ACE2-algae-robot in TAP, DI water, drinking water, and river water containing 1×10^8 VG of the virus, (n = 3; mean ± s.d.). (c) Effect of the ACE2-algae-robot density on the efficiency of virus removal in drinking water. (d) Representative fluorescent images of NL-20 cells infected with virus treated by different densities of the ACE2-algae-robot. Scale bar: 100 μm. (e) Efficiency of the virus removal in drinking water with the treatment of the ACE2-algae-robot, bare algae, static ACE2-algae, or cell wall deficient algae. (f) Representative fluorescent images of NL-20 cells infected with the virus treated by the ACE2-algae-robot, bare algae, static ACE2-algae, and cell wall deficient algae. Scale bar: 100 μm. (g) Kinetic profile of the virus removal efficiency in drinking water with the treatment of the ACE2-algae-robot, bare algae, and static ACE2-algae (n = 3; mean ± s.d.). (h) Representative fluorescent images of NL-20 cells infected with the virus, which is treated by the ACE2-algae-robot for different times (0, 1, 2, and 4 h). Scale bar: 100 μm.

incubation in pseudovirus contaminated water samples upon ACE2-algae-robot treatment, confirming the highly effective pseudovirus removal by the robot. In comparison, without the ACE2-algae-robot treatment, the cells displayed bright fluorescence, reflecting the pseudovirus entry and significant expression of fluorescent protein in the host cells. Figure 4b and S6 show the motion behavior (speed and lifespan) of the ACE2-algae-robot in various water matrices containing the SARS-CoV-2 pseudovirus. The biohybrid microrobot displays similar speed in these aqueous media, which is similar to that observed in Figure 2b without the pseudovirus, indicating that the presence of the pseudovirus does not hamper the movement of the ACE2-algae-robot.

Next, we investigated the effect of ACE2-algae-robot density on the removal efficiency of SARS-CoV-2 pseudovirus from drinking water. As shown in Figure 4c, the results demonstrated a gradual increase of the removal efficiency, 19% to 90%, upon increasing ACE2-algae-robot concentrations from 5×10^4 mL^{-1} to 5×10^7 mL^{-1}. The pseudovirus removal efficiency was also visualized by fluorescent imaging. As expected, the highest robot concentration resulted in a minimal fluorescent virus signal (Figure 4d and S7). The ACE2-algae-robot also offers significant improvement (89%) in the removal of SARS-CoV-2 pseudovirus compared with control groups, including static ACE2-algae (31%), bare algae (63%), and cell-wall deficient algae (21%) (Figure 4e). These experiments

https://doi.org/10.1021/jacs.1c04933
J. Am. Chem. Soc. XXXX, XXX, XXX−XXX

were performed by immersing 2.5×10^5 of algae in a 50 μL drinking water sample containing 2×10^9 VG ml^{-1} (VG: viral genomes) pseudovirus for 16 h. In the control experiments, the viral binding capability of the bare algae is possibly attributed to both biosorption[30] and physical entrapment of the virus into the porous structure of the algae cell wall.[31] The fluorescence images in Figure 4f and Figure S8 illustrate the minimal fluorescent virus signal with the ACE2-algae-robot treatment, corresponding to the virus removal efficiency data of Figure 4e. Furthermore, we evaluated and compared the virus removal kinetic profiles in drinking water treated with the ACE2-algae-robot, bare algae, or static ACE2-algae (Figure 4g). These data illustrate that the ACE2-algae-robot can effectively remove 85% of pseudovirus after 4 h treatment, compared to 60% and 18% for bare algae and static ACE2-algae, respectively. Therefore, each ACE2-algae-robot can bind to ~340 VG of virus. Such results indicate the significant contributions of both the ACE2 receptor for virus targeting and the fast microrobot motion for contacting the virus toward highly efficient viral binding and removal. The representative fluorescence images also show the progression of the viral infection over time with samples treated with the ACE2-algae-robot (Figure 4h and Figure S9). Furthermore, the ACE2-algae-robot can be reused to reach 90% viral removal efficiency after five repeated cycles (Figure S10). A post-treatment of the ACE2-algae-robot by flocculant was performed to clean the robot in the water sample (Figure S11). The flocculant can isolate the ACE2-algae-robot from the water matrices without affecting the virus removal efficiency, holding considerable potential for practical future applications.

CONCLUSIONS

In summary, we have developed an effective biohybrid microrobotic method to actively remove the SARS-CoV-2 spike protein and pseudovirus from various water matrices using ACE2 receptor-modified microalgae. The ACE2-algae-robot can be readily fabricated by an efficient click chemistry approach, without compromising the motion behavior of algae and the function of the ACE2 receptor. The resulting ACE2-algae-robot displays excellent motion ability in various water matrices and offers considerable potential to clean contaminated water samples. The binding and removal capability of the ACE2-algae-robot were demonstrated and characterized using both SARS-CoV-2 spike protein and SARS-CoV-2 pseudovirus, resulting in 95% and 89% removal efficiency, respectively, at the experimental conditions. Given the high concentration of viral load (2×10^9 VG ml^{-1}) in our experiment, the removal efficiency of 89% and binding capability of ~340 VG algae^{-1} represent a high efficacy compared to the traditional wastewater viral treatments.[32] The enhanced removal of the viral spike protein and pseudovirus is attributed to the continuous self-propulsion of the ACE2-algae-robot and corresponding mixing and collision with the target protein and virus. The reusability and post-treatment of the microrobot were also studied, demonstrating considerable promise for removing waterborne pathogenic viruses from contaminated water. Although current platform can reach 89% viral removal, it is difficult to directly convert viral concentration in wastewater to disease prevalence in hosts.[33] However, any reduction of viral load would have a positive correlation with the control of viral infectivity and the illness of patients.[34] The algae microrobots are expected to have greater mobility and longer lifetime in an open wastewater reservoir when compared to a confined test tube and thus hold considerable potential for future scaling-up applications. Given that new emerging SARS-CoV-2 variants show a similar binding mechanism and higher binding affinity with the ACE2 receptor,[35,36] the functionalized algae microrobotic platform is expected to efficiently remove different virus variants from wastewater. Overall, by relying on click chemistry to attach protein receptors onto natural algae surfaces, such a functionalized algae-based microrobot offers an attractive strategy for a variety of environmental remediation applications.

ASSOCIATED CONTENT

Supporting Information

The Supporting Information is available free of charge at https://pubs.acs.org/doi/10.1021/jacs.1c04933.

Flow cytometry histograms; SEM images of the ACE2-algae-robot before and after contact with the SARS-CoV-2 pseudovirus; representative microscopy bright-field and fluorescence images of bare algae incubated with DBCO-PEG$_4$-NHS ester and labeled with an azido-based fluorescence probe; mean speed distribution of ACE2-algae-robot in drinking and river water containing the SARS-CoV-2 spike protein; photographs of the ACE-algae-robot and static ACE2-algae after 6 h incubation with SARS-CoV-2 spike protein; speed comparison of ACE2-algae-robots before and after 24 h motion in drinking and river water containing the SARS-CoV-2 pseudovirus; representative microscopy brightfield and fluoresence images of NL-20 cells infected with virus treated by different densities of the ACE2-algae-robot, by the ACE2-algae-robot, bare algae, static ACE2-algae, and cell-wall deficient algae, and by the ACE2-algae-robot for different times, efficiency of virus removal after ACE2-algae-robot reutilization; and efficiency of the virus removal from drinking water after employing ACE2-algae-robot with post-treatment by the flocculant (PDF)

Effect of the algae functionalization upon its swimming behavior (MP4)

Motion of the ACE2-algae-robot in different aqueous media (MP4)

Speed of ACE2-algae-robot at different time points in drinking water and river water (MP4)

Representative optical trajectories of the movement of ACE2-algae-robot over 2.5 s motion in drinking water (MP4)

Representative optical trajectories of the movement of ACE2-algae-robot over 2.5 s motion in river water (MP4)

AUTHOR INFORMATION

Corresponding Authors

Liangfang Zhang − *Department of NanoEngineering and Chemical Engineering Program, University of California San Diego, La Jolla, California 92093, United States;* orcid.org/0000-0003-0637-0654; Email: zhang@ucsd.edu

Joseph Wang − *Department of NanoEngineering and Chemical Engineering Program, University of California San Diego, La Jolla, California 92093, United States;* orcid.org/0000-0002-4921-9674; Email: josephwang@ucsd.edu

https://doi.org/10.1021/jacs.1c04933
J. Am. Chem. Soc. XXXX, XXX, XXX−XXX

Authors

Fangyu Zhang − *Department of NanoEngineering and Chemical Engineering Program, University of California San Diego, La Jolla, California 92093, United States;* orcid.org/0000-0002-6522-5230

Zhengxing Li − *Department of NanoEngineering and Chemical Engineering Program, University of California San Diego, La Jolla, California 92093, United States*

Lu Yin − *Department of NanoEngineering and Chemical Engineering Program, University of California San Diego, La Jolla, California 92093, United States*

Qiangzhe Zhang − *Department of NanoEngineering and Chemical Engineering Program, University of California San Diego, La Jolla, California 92093, United States*

Nelly Askarinam − *Department of NanoEngineering and Chemical Engineering Program, University of California San Diego, La Jolla, California 92093, United States*

Rodolfo Mundaca-Uribe − *Department of NanoEngineering and Chemical Engineering Program, University of California San Diego, La Jolla, California 92093, United States*

Farshad Tehrani − *Department of NanoEngineering and Chemical Engineering Program, University of California San Diego, La Jolla, California 92093, United States*

Emil Karshalev − *Department of NanoEngineering and Chemical Engineering Program, University of California San Diego, La Jolla, California 92093, United States*

Weiwei Gao − *Department of NanoEngineering and Chemical Engineering Program, University of California San Diego, La Jolla, California 92093, United States*

Complete contact information is available at: https://pubs.acs.org/10.1021/jacs.1c04933

Author Contributions

#F.Z. and Z.L. contributed equally to this work.

Funding

This work was supported by the Defense Threat Reduction Agency Joint Science and Technology Office for Chemical and Biological Defense under Grant HDTRA1-21-1-0010 and the National Science Foundation Grant DMR-1904702.

Notes

The authors declare no competing financial interest.

REFERENCES

(1) Zhang, R.; Li, Y.; Zhang, A. L.; Wang, Y.; Molina, M. J. Identifying airborne transmission as the dominant route for the spread of COVID-19. *Proc. Natl. Acad. Sci. U. S. A.* **2020**, *117*, 14857−14863.

(2) Wu, Y.; Guo, C.; Tang, L.; Hong, Z.; Zhou, J.; Dong, X.; Yin, H.; Xiao, Q.; Tang, Y.; Qu, X.; Kuang, L.; Fang, X.; Mishra, N.; Lu, J.; Shan, H.; Jiang, G.; Huang, X. Prolonged presence of SARS-CoV-2 viral RNA in faecal samples. *Lancet Gastroenterol. Hepatol.* **2020**, *5*, 434−435.

(3) Randazzo, W.; Truchado, P.; Cuevas-Ferrando, E.; Simón, P.; Allende, A.; Sánchez, G. SARS-CoV-2 RNA in wastewater anticipated COVID-19 occurrence in a low prevalence area. *Water Res.* **2020**, *181*, 115942.

(4) Haramoto, E.; Malla, B.; Thakali, O.; Kitajima, M. First environmental surveillance for the presence of SARS-CoV-2 RNA in wastewater and river water in Japan. *Sci. Total Environ.* **2020**, *737*, 140405.

(5) Guerrero-Latorre, L.; Ballesteros, I.; Villacrés-Granda, I.; Granda, M. G.; Freire-Paspuel, B.; Ríos-Touma, B. SARS-CoV-2 in river water: Implications in low sanitation countries. *Sci. Total Environ.* **2020**, *743*, 140832.

(6) Wu, F.; Zhang, J.; Xiao, A.; Gu, X.; Lee, W. L.; Armas, F.; Kauffman, K.; Hanage, W.; Matus, M.; Ghaeli, N.; Endo, N.; Duvallet, C.; Poyet, M.; Moniz, K.; Washburne, A. D.; Erickson, T. B.; Chai, P. R.; Thompson, J.; Alm, E. J. SARS-CoV-2 titers in wastewater are higher than expected from clinically confirmed cases. *Msystems* **2020**, *5*, e00614−e00620.

(7) Foladori, P.; Cutrupi, F.; Segata, N.; Manara, S.; Pinto, F.; Malpei, F.; Bruni, L.; La Rosa, G. SARS-CoV-2 from faeces to wastewater treatment: what do we know? A review. *Sci. Total Environ.* **2020**, *743*, 140444.

(8) Bogler, A.; Packman, A.; Furman, A.; Gross, A.; Kushmaro, A.; Ronen, A.; Dagot, C.; Hill, C.; Vaizel-Ohayon, D.; Morgenroth, E. Rethinking wastewater risks and monitoring in light of the COVID-19 pandemic. *Nat. Sustainability* **2020**, *3*, 981−990.

(9) Zhang, Q.; Dong, R.; Wu, Y.; Gao, W.; He, Z.; Ren, B. Light-Driven Au-WO3@C Janus Micromotors for Rapid Photodegradation of Dye Pollutants. *ACS Appl. Mater. Interfaces* **2017**, *9*, 4674−4683.

(10) Liang, C.; Zhan, C.; Zeng, F.; Xu, D.; Wang, Y.; Zhao, W.; Zhang, J.; Guo, J.; Feng, H.; Ma, X. Bilayer Tubular Micromotors for Simultaneous Environmental Monitoring and Remediation. *ACS Appl. Mater. Interfaces* **2018**, *10*, 35099−35107.

(11) Vilela, D.; Parmar, J.; Zeng, Y.; Zhao, Y.; Sánchez, S. Graphene-based microbots for toxic heavy metal removal and recovery from water. *Nano Lett.* **2016**, *16*, 2860−2866.

(12) Maric, T.; Mayorga-Martinez, C. C.; Khezri, B.; Nasir, M. Z. M.; Chia, X.; Pumera, M. Nanorobots Constructed from Nanoclay: Using Nature to Create Self-Propelled Autonomous Nanomachines. *Adv. Funct. Mater.* **2018**, *28*, 1802762.

(13) Mou, F.; Pan, D.; Chen, C.; Gao, Y.; Xu, L.; Guan, J. Magnetically Modulated Pot-Like MnFe2O4Micromotors: Nanoparticle Assembly Fabrication and their Capability for Direct Oil Removal. *Adv. Funct. Mater.* **2015**, *25*, 6173−6181.

(14) Hoop, M.; Shen, Y.; Chen, X. Z.; Mushtaq, F.; Iuliano, L. M.; Sakar, M. S.; Petruska, A.; Loessner, M. J.; Nelson, B. J.; Pané, S. Magnetically driven silver-coated nanocoils for efficient bacterial contact killing. *Adv. Funct. Mater.* **2016**, *26*, 1063−1069.

(15) Lin, Z.; Gao, C.; Wang, D.; He, Q. Bubble-propelled Janus Gallium/Zinc Micromotors for Active Treatment of Bacterial Infection. *Angew. Chem., Int. Ed.* **2021**, *60*, 8750−8754.

(16) Kong, L.; Ambrosi, A.; Nasir, M. Z. M.; Guan, J.; Pumera, M. Self-Propelled 3D-Printed "Aircraft Carrier" of Light-Powered Smart Micromachines for Large-Volume Nitroaromatic Explosives Removal. *Adv. Funct. Mater.* **2019**, *29*, 1903872.

(17) Li, J.; Singh, V. V.; Sattayasamitsathit, S.; Orozco, J.; Kaufmann, K.; Dong, R.; Gao, W.; Jurado-Sanchez, B.; Fedorak, Y.; Wang, J. Water-driven micromotors for rapid photocatalytic degradation of biological and chemical warfare agents. *ACS Nano* **2014**, *8*, 11118−11125.

(18) Gao, W.; Wang, J. The environmental impact of micro/nanomachines: a review. *ACS Nano* **2014**, *8*, 3170−3180.

(19) Parmar, J.; Vilela, D.; Villa, K.; Wang, J.; Sanchez, S. Micro- and Nanomotors as Active Environmental Microcleaners and Sensors. *J. Am. Chem. Soc.* **2018**, *140*, 9317−9331.

(20) Zhang, Y.; Yan, K.; Ji, F.; Zhang, L. Enhanced Removal of Toxic Heavy Metals Using Swarming Biohybrid Adsorbents. *Adv. Funct. Mater.* **2018**, *28*, 1806340.

(21) Soto, F.; Lopez-Ramirez, M. A.; Jeerapan, I.; Esteban-Fernández de Ávila, E. F.; Mishra, R. K.; Lu, X.; Chai, I.; Chen, C.; Kupor, D.; Nourhani, A.; Wang, J. Rotibot: Use of Rotifers as Self-Propelling Biohybrid Microcleaners. *Adv. Funct. Mater.* **2019**, *29*, 1900658.

(22) Palagi, S.; Fischer, P. Bioinspired microrobots. *Nat. Rev. Mater.* **2018**, *3*, 113−124.

(23) Lee, J.-H.; Choi, M.; Jung, Y.; Lee, S. K.; Lee, C.-S.; Kim, J.; Kim, J.; Kim, N. H.; Kim, B.-T.; Kim, H. G. A novel rapid detection for SARS-CoV-2 spike 1 antigens using human angiotensin converting enzyme 2 (ACE2). *Biosens. Bioelectron.* **2021**, *171*, 112715.

(24) Huang, Y.; Yang, C.; Xu, X.-f.; Xu, W.; Liu, S.-w. Structural and functional properties of SARS-CoV-2 spike protein: potential antivirus

drug development for COVID-19. *Acta Pharmacol. Sin.* **2020**, *41*, 1141−1149.
(25) Glasgow, A.; Glasgow, J.; Limonta, D.; Solomon, P.; Lui, I.; Zhang, Y.; Nix, M. A.; Rettko, N. J.; Zha, S.; Yamin, R.; Kao, K.; Rosenberg, O. S.; Ravetch, J. V.; Wiita, A. P.; Leung, K. K.; Lim, S. A.; Zhou, X. X.; Hobman, T. C.; Kortemme, T.; Wells, J. A. Engineered ACE2 receptor traps potently neutralize SARS-CoV-2. *Proc. Natl. Acad. Sci. U. S. A.* **2020**, *117*, 28046−28055.
(26) Wollmann, F.; Dietze, S.; Ackermann, J. U.; Bley, T.; Walther, T.; Steingroewer, J.; Krujatz, F. Microalgae wastewater treatment: biological and technological approaches. *Eng. Life Sci.* **2019**, *19*, 860−871.
(27) Yasa, O.; Erkoc, P.; Alapan, Y.; Sitti, M. Microalga-Powered Microswimmers toward Active Cargo Delivery. *Adv. Mater.* **2018**, *30*, 1804130.
(28) Silflow, C. D.; Lefebvre, P. A. Assembly and motility of eukaryotic cilia and flagella. Lessons from Chlamydomonas reinhardtii. *Plant Physiol.* **2001**, *127*, 1500−1507.
(29) Xiong, H.-L.; Wu, Y.-T.; Cao, J.-L.; Yang, R.; Liu, Y.-X.; Ma, J.; Qiao, X.-Y.; Yao, X.-Y.; Zhang, B.-H.; Zhang, Y.-L. Robust neutralization assay based on SARS-CoV-2 S-protein-bearing vesicular stomatitis virus (VSV) pseudovirus and ACE2-overexpressing BHK21 cells. *Emerging Microbes Infect.* **2020**, *9*, 2105−2113.
(30) Bhatt, A.; Arora, P.; Prajapati, S. K. Can Algal Derived Bioactive Metabolites Serve as Potential Therapeutics for the Treatment of SARS-CoV-2 Like Viral Infection? *Front. Microbiol.* **2020**, *11*, 596374.
(31) Goodenough, U. W.; Heuser, J. E. The Chlamydomonas cell wall and its constituent glycoproteins analyzed by the quick-freeze, deep-etch technique. *J. Cell Biol.* **1985**, *101*, 1550−1568.
(32) Carducci, A.; Battistini, R.; Rovini, E.; Verani, M. Viral removal by wastewater treatment: monitoring of indicators and pathogens. *Food Environ. Virol.* **2009**, *1*, 85−91.
(33) Larsen, D. A.; Wigginton, K. R. Tracking COVID-19 with wastewater. *Nat. Biotechnol.* **2020**, *38*, 1151−1153.
(34) Goyal, A.; Reeves, D. B.; Thakkar, N.; Famulare, M.; Cardozo-Ojeda, E. F.; Mayer, B. T.; Schiffer, J. T. Slight reduction in SARS-CoV-2 exposure viral load due to masking results in a significant reduction in transmission with widespread implementation. *Sci. Rep.* **2021**, *11*, 11838.
(35) Zhou, D.; Dejnirattisai, W.; Supasa, P.; Liu, C.; Mentzer, A. J.; Ginn, H. M.; Zhao, Y.; Duyvesteyn, H. M.; Tuekprakhon, A.; Nutalai, R.; et al. Evidence of escape of SARS-CoV-2 variant B. 1.351 from natural and vaccine-induced sera. *Cell* **2021**, *184*, 2348−2361.
(36) Khan, A.; Zia, T.; Suleman, M.; Khan, T.; Ali, S. S.; Abbasi, A. A.; Mohammad, A.; Wei, D. Q. Higher infectivity of the SARS-CoV-2 new variants is associated with K417N/T, E484K, and N501Y mutants: An insight from structural data *J. Cell. Physiol.* **2021**, Article ASAP, DOI: 10.1002/jcp.30367 (accessed 2021-06-22).

https://doi.org/10.1021/jacs.1c04933
J. Am. Chem. Soc. XXXX, XXX, XXX−XXX